Terahertz Wireless Links Using Diffuse Scattering From Rough Surfaces

Jianjun Ma, Rabi Shrestha, Wei Zhang, Lothar Moeller, and Daniel M. Mittleman, *Fellow, IEEE*

***Abstract*—We describe measurements of the diffuse bistatic scattering of a modulated terahertz beam incident on five metallic rough surfaces, to investigate the implications of surface roughness for non-line-of-sight (NLOS) wireless data links at frequencies at and above 100 GHz. The measurements were performed using transmitter and receiver modules, operating at several frequencies from 100 to 400 GHz. We investigate the dependence of the scattering patterns on surface roughness parameters, including rms height and correlation length. The results are consistent with numerical models for scattering from a rough surface. They support the design of bistatic methods for future multiple antenna systems, remote sensing, imaging, and localization in the terahertz range. We demonstrate for the first time that data links which incorporate an NLOS reflection in a nonspecular direction can be established at frequencies above 100 GHz, with low bit error rates.**

***Index Terms*—Diffuse scattering, reflection, rough surface, terahertz (THz) wireless communications.**

I. Introduction

THE increasing requirements of huge data traffic [1], [2] forces future wireless networks to consider the use of higher carrier frequencies in the terahertz (THz) range, as they offer much wider bandwidth for supporting high data rates. This approach can address the looming capacity limitations of both existing 4G and near-term 5G systems, and will enable new applications such as indoor ultrahigh speed wireless communications [3], intrabody sensors [4], and secure data transfer [5]. Although THz frequencies are evidently a good candidate for future point-to-point communications, these directional links exhibit significant susceptibility to blockage due to human bodies and other objects [6]. One solution under active investigation is to employ steerable antennas to establish a non-line-of-sight (NLOS) link [7], [8]. We have recently demonstrated that a typical indoor surface (e.g., a painted cinderblock wall) can produce a directional reflected beam for establishing a link with tolerable additional loss, at least up to 200 GHz [9]. Since this result relied on a specular reflection (i.e., angle of reflection = angle of incidence) from the rough surface, this demonstration still represented essentially a line-of-sight (LOS) link. The possibility of a true NLOS link, which relies on diffuse scattering of radiation along a nonspecular ray path, has yet to be studied at these frequencies.

At lower frequencies, scattering effects due to reflection are always a key factor affecting wireless link performance. Many such measurements have been described, for both indoor and outdoor links, with carrier frequencies ranging from 0.9 to 73 GHz [10]–[18]. One key observation in these studies was a larger RMS delay spread for NLOS channels. These NLOS channels can be exploited usefully, because they permit many different pointing angles for establishing links with optimized SNR and delay spread. In the THz range (above 100 GHz), the situation may be somewhat different, as NLOS paths will become increasingly sparse and lossy. The ultimate impact of these changes on link performance remains unknown. This article highlights the need for further investigation into these phenomena at higher frequencies to support the development of techniques and models for future wireless networks.

Some studies of scattering phenomena at THz frequency have been reported previously. These works include studies of multiple scattering from dense random media (e.g., [19], [20]) and scattering upon reflection by rough surfaces (e.g., [21]–[24]). These measurements have usually been performed using THz time domain spectroscopy, or using a vector network analyzer. To our knowledge, studies of NLOS links above 100 GHz with data transmission have not yet been reported.

In this article, we investigate the performance of a data link which relies on a path that incorporates a single scattering from a rough surface. These home-made rough surfaces are used as models to provide a controlled scattering situation. We employ a THz source that produces a signal with an amplitude-shift keying modulation at a data rate of 1 Gb/s, at carrier frequencies of 100, 200, 300, and 400 GHz. We characterize the link using both received power and bit error rate, via angle- and polarization-dependent measurements. We use the integral equation method (IEM) as proposed by Fung [25] to predict the properties of the scattered wave front, and we compare with the measured polarimetric bistatic response of the rough surfaces.

Manuscript received March 26, 2019; revised May 28, 2019; accepted July 29, 2019. Date of publication August 5, 2019; date of current version September 2, 2019. This work was supported in part by the W. M. Keck Foundation and in part by the US National Science Foundation. *(Corresponding author: Daniel M. Mittleman.)*

J. Ma is with Brown University, Providence, RI 02912 USA, and also with the Beijing Institute of Technology, Beijing 100081, China (e-mail: 6120190050@bit.edu.cn).

R. Shrestha, W. Zhang, and D. M. Mittleman are with Brown University, Providence, RI 02912 USA (e-mail: rabi_shrestha@brown.edu; wei_zhang@brown.edu; daniel_mittleman@brown.edu).

L. Moeller is with the New Jersey Institute of Technology, Newark, NJ 07102 USA (e-mail: lmoeller@subcom.com).

Color versions of one or more of the figures in this article are available online at http://ieeexplore.ieee.org.

Digital Object Identifier 10.1109/TTHZ.2019.2933166

2156-342X © 2019 IEEE. Personal use is permitted, but republication/redistribution requires IEEE permission.
See http://www.ieee.org/publications_standards/publications/rights/index.html for more information.

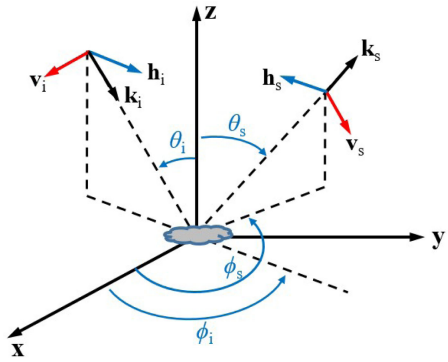

Fig. 1. Basic geometry of scattering at a rough surface.

II. Scattering Theory

An electromagnetic wave incident on a rough surface generally scatters in all directions. Consider the general scattering geometry shown in Fig. 1(a), where the wave bounces off a surface with an incident angle of θ_i. Here, we just consider one-bounce scattering; the effects of multiple scattering have been considered at lower frequencies [16]. When the surface is smooth, the wave with polarization q (where $q = h$ or v) is reflected along the specular direction as determined by Snell's law, and no scattering occurs. This component is called the coherent component with a uniform phase front; its reflected power is related to the incident power as $P_q^s = \Gamma^q_{\text{smooth}}\ P_q^i$ as derived from the Fresnel equations. Here, Γ^q_{smooth} is the q-polarized Fresnel reflectivity of the flat surface; P_q^i, P_q^r are the incident and reflected power, respectively. When the surface is rough, the scattering pattern also includes an incoherent component, with power propagating along all other directions. In this case, the coherent power along the specular direction is determined by a modified reflectivity $\Gamma^q_{\text{rough}} = \rho.\Gamma^q_{\text{smooth}}$ with ρ as the scattering loss factor, $\rho < 1$ [26]. In a regime of intermediate roughness, both the coherent and incoherent components can contain significant fractions of the incident wave's power. However, when the roughness increases further and further, the incoherent component dominates along all directions while the coherent component becomes negligible (i.e., $\rho << 1$).

To characterize surface roughness, two fundamental parameters are usually considered. The standard deviation of the surface height variation (rms height) σ characterizes the vertical roughness (i.e., perpendicular to the surface), and the surface correlation length L_c indicates the correlation between the heights of adjacent points along the surface [27]. L_c can be regarded as a measure of horizontal roughness of a surface. For small values of the correlation length, the surface is very discontinuous with many irregularities, whereas larger values indicate a more smoothly continuous variation. A third parameter is the rms slope m, which can be used to assess the relative contribution of multiple scattering effects. Here, we neglect the effects of multiple scattering, so this parameter is not relevant for the present discussion.

In order to evaluate whether a surface is electromagnetically smooth or not, the Rayleigh roughness criterion, which relies on the attenuation of the coherent intensity owing to the rough surface, is useful as a first-order classifier. Here, we consider a common situation for the millimeter and terahertz region in which the wavelength λ is of the order of the rms height σ. In this situation, we must use a more stringent criterion, known as the Fraunhofer criterion, as described by Ulaby [28]. This criterion states that the surface may be considered smooth when the phase difference between two rays scattered from separate points on the surface $\Delta\phi < \pi/8$. This corresponds to $\sigma < \lambda/(32\cos\theta_i)$ for a random natural surface.

We note that the general problem of the scattering of electromagnetic waves is still not solved completely and no exact closed-form solutions exist. Yet, because of the ubiquity of the problem, there have been many studies investigating these effects [24], [26], [29]–[33]. In one recent example, Ju *et al.* employed a dual-lobe directive scattering model and obtained good agreement with measured peak power in the specular direction after reflection [24]. Here, we use the modified IEM, which is among the most commonly used theories for the modeling of diffuse scattering [25], [27], [34]–[36]. It permits the computation of the radiated field from a rough surface by integrating the total bistatic scattering over the upper hemisphere above the rough surface. This model employs four correlation functions and multiple roughness scales to characterize the surface height profile. It can be used to compute the backscattering and bistatic scattering coefficient of a random surface with any specified degree of roughness for any combination of receive and transmit wave polarizations. An exponential correlation function with different rate parameter can be used to describe the surface height profile. Here, the rate parameter indicates how often on average the scattering events occur. Different from exponential and Gaussian function, the two fitting parameters (rate parameter and correlation distance of the surface) can provide greater flexibility in matching the model based on measured surface height profiles. Fung [27] demonstrated that, in practice, scattering is more sensitive to the surface correlation length than to the surface height statistics.

As mentioned above, the bistatic scattering pattern consists of a coherent component along the specular direction and incoherent component along all other directions. So the total scattering coefficient consists of a coherent component $\sigma^0_{qq\_\text{coh}}(\theta_i)$ and an incoherent component $\sigma^0_{qq\_\text{inc}}(\theta_i,\phi_i;\theta_s,\phi_s)$ as follows:

$$\sigma^0_{qq}(\theta_i,\phi_i;\theta_s,\phi_s) = \sigma^0_{qq\_\text{coh}}(\theta_i) + \sigma^0_{qq\_\text{inc}}(\theta_i,\phi_i;\theta_s,\phi_s)\,. \tag{1}$$

In our measurements, we consider the case where the incident angle $\theta_i = 45^\circ$; the azimuth angles $\phi_i = \phi_s = 0^\circ$ for bistatic configuration. The scattering angle θ_s (i.e., the angle at which the detector is located) changes from 0° to 90°. The subscript qq ($q = v$ or h) indicates the orientation of the polarization; the first index refers to the orientation of the receive antenna and the second one refers to the polarization of the transmitted wave. This notation will be used throughout this article.

The incoherent component can be obtained using the IEM model, which gives a simple solution to describe the scattering behavior caused by the rough surface. In the model, the surface field is separated into the Kirchhoff field and the complementary field, and the bistatic scattering coefficients can be summarized

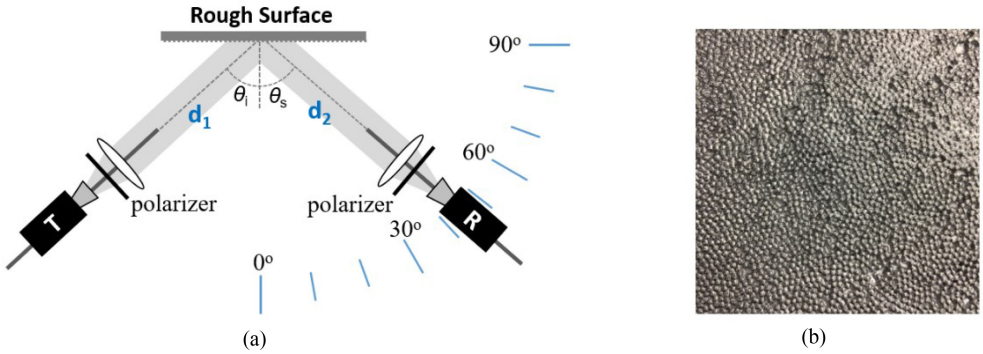

Fig. 2. (a) Configuration of the measurement system. (b) Picture of Sample I in Table I.

as follows [27]:

$$\sigma_{qq}^{0} = \frac{k^2}{2}\exp\left[-\sigma^2\left(k_z^2 + k_{sz}^2\right)\right]\sum_{n=1}^{\infty}\frac{\sigma^{2n}}{n!}\left(I_{qp}^{n}I_{rs}^{n*}\right)W^{(n)} \quad (2)$$

where $W^{(n)}$ is the roughness spectrum of the surface related to the nth power of the surface correlation function by the Fourier transform as follows:

$$W^{(n)} = \int_0^{\infty}\rho^n(\xi)\,J_0(k\xi)\,\xi d\xi \quad (3)$$

with $\rho(\xi)$ as the correlation function and $J_0(k\xi)$ as the first spherical Bessel function

$$I_{\alpha\beta}^{n} = (k_{sz}+k_z)^n f_{\alpha\beta}\exp(-\sigma^2 k_{sz}k_z) + \frac{(k_{sz})^n F_{\alpha\beta}(-k_x,-k_y) + (k_z)^n F_{\alpha\beta}(-k_{sx},-k_{sy})}{2} \quad (4)$$

where $f_{\alpha\beta}$ is the Kirchhoff field coefficient and $F_{\alpha\beta}$ is the complementary field coefficient, which are correlated to the Kirchhoff and complementary fields. The parameters k_x, k_y, k_z, k_{sx}, k_{sy}, k_{sz} are the Cartesian components of the wave vectors k and k_s. So, the total scattering coefficient σ_{qq}^{0} depends on the rms height and the surface correlation length, as well as the dielectric constant of the surface material ε through the Fresnel reflection coefficients [25], [27], [34].

The Friis transmission formula is used to calculate the received power by integrating this cross section, as in a distributed target bistatic radar equation

$$P_r = P_t\frac{G_0^2\lambda^2}{(4\pi)^3}\iint\frac{dA}{R_r^2R_t^2}\cdot\sigma_{qq}^{0}(\theta_i,\phi_i;\theta_s,\phi_s)\,. \quad (5)$$

Here, G_0 is the antenna gain for both transmitter and receiver, and A is the illuminated area on the rough surface, over which the integral is performed. R_t and R_r refer to the distances from the rough surface to the transmitter and receiver, respectively.

The IEM model has been employed to characterize backscattering effects by several authors, by setting the azimuth angle $\phi_s = 180^{\circ}$ in (5). For example, in [37], the model shows good agreement with measured backscattering behavior of a rough aluminum plate at 160 GHz, 240 GHz, and 1.55 THz. It has also been used to calculate the surface scattering behavior of a multilayer dielectric material [29].

TABLE I
METALLIC SAMPLE PARAMETERS

Sample	Ball diameter (mm)	RMS height (mm)	Correlation length (mm)
I	0.7	0.30	16
II	1.0	0.72	18
III	1.5	0.38	28
IV	2.0	0.50	22
V	3.0	0.77	19

III. MEASUREMENTS

Our THz source is based on a frequency-multiplier-chain (Virginia Diodes), which consists of several cascaded frequency doublers and triplers, all based on Schottky diodes. A 1 Gb/s non-return-to-zero (NRZ) format signal is generated by a pulse pattern generator. A duobinary modulation technique is utilized for driving the THz, which enables signaling at high data rate, with relatively compact spectrum and higher output power compared to regular NRZ modulation by applying phase coding and pulse broadening. A quasi-Gaussian low-pass filter (LPF) with about 500 MHz 3 dB bandwidth is then applied to reduce the spectral width of the signal. This signal is launched into the intermediate frequency port of a double-balanced mixer, where the data modulates the output of a frequency synthesizer that is connected to the local oscillator port. The data modulates the THz radiation which is coupled to free space by a horn antenna.

The output of the horn is collimated by a THz lens (beam diameter ~50 mm) with short focal length (~75 mm) and transmitted through air. An identical THz lens couples the beam into a receiver horn similar to the transmitter antenna, whose output is connected to a zero biased Schottky diode. The Schottky diode's output is amplified by about 52 dB using two amplifiers and filtered by a quasi-Gaussian LPF with 1.5 GHz 3 dB bandwidth. A 6 dB electrical power splitter launches one output to an RF power meter and the other to a bit error rate tester (BERT). The

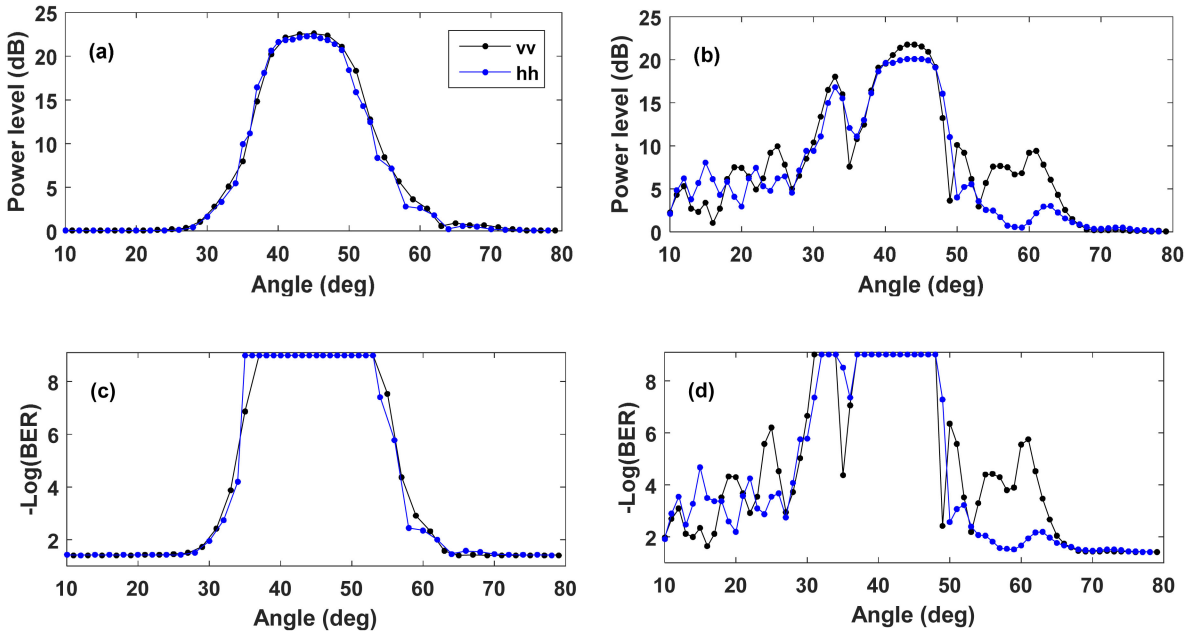

Fig. 3. Received power and BER pattern measurements as a function of the scattering angle θ_s after reflection by [(a), (c)] smooth surface and [(b), (d)] sample V with a carrier frequency of 100 GHz. Measurements were performed at a fixed incidence angle $\theta_i = 45^{\circ}$.

BERT saturates at an error rate of 10^{-9}, which we consider to be error-free operation. Both the Tx and Rx antennas are mounted at a height of 0.4 m above the table, which is covered by absorbers to suppress unwanted reflections from the table surface. The system gains and half-power-beam-widths are specified in [9].

Fig. 2(a) shows our experimental configuration used to explore the diffuse scattering from rough metal surfaces. The schematic illustrates the Tx and Rx subassemblies, with Teflon lenses, directed toward a spot on the surface. The distance from the Tx and Rx antenna to the surface is constant ($d_1 = 0.5$ m and $d_2 = 1$ m). The antennas always point to the surface for all frequencies, and a direct LOS free-space calibration was performed at each measured frequency at a Tx–Rx separation distance of 1.5 m ($d_1 + d_2 = 1.5$ m). To assure the linear behavior of the SBD, we used calibrated attenuators after the Tx antenna. We mount the receiver on a movable rotator which permits it to rotate along an arc with its center at the rough surface. By scanning the detector along this arc, we map the angular distribution of the beam arriving at the receiver horn. The detector angle is optimized to ensure accurate pointing, prior to each scan. The incident angle θ_i is restricted to 45°, azimuth angle $\phi_i = \phi_s = 0^{\circ}$, while the detection angle θ_s was varied in most cases between 10° and 80° with a step of 1°. Scattering in the backward direction ($\phi_s = 180^{\circ}$) is not measured in this article due to the fact that the transmitter obstructs the view of the receiver.

We fabricated a set of scattering metallic samples with rough surfaces. As shown in Fig. 2(b), 10 000 small steel balls with identical diameter were poured randomly onto a smooth steel surface with a thin layer of glue on top of it. Then, the surfaces were painted by silver paint. This paint has a dielectric constant $\varepsilon = 2.6 \times 10^5 - j1.0 \times 10^6$ [38]–[40], when it is dried. We fabricate five different samples, using steel balls with different diameters ranging from 0.7 to 3.0 mm. We measured height profiles of the surfaces by using a mechanical up-down height meter. The profiles were collected by positioning a movable needle above the surface, without perturbing the surface, while performing horizontal scans at a step smaller than λ/10. The rms height and correlation length are derived from the measured height profiles and are shown in Table I.

IV. Results and Discussion

In Fig. 3, we show the scattered power and BER pattern measured when a surface is illuminated with a 100 GHz data stream. This figure compares the results from a smooth surface to those from Sample V. The scattering pattern is shown for both vertical and horizontal input polarization. We observe that the scattering pattern is broadened with a strong coherent component along the specular direction when the surface is rough. The angular broadening is due to the presence of the incoherent component, which gives rise to radiation along directions other than the specular direction. This result illustrates that a data link can be established when the angle of reflection is different from the angle of incidence, as a result of the incoherent component scattered from the rough surface. To our knowledge, this is the first demonstration of a true nonspecular NLOS data link by rough surfaces at terahertz frequencies.

We also note that the difference in power level between the *vv* and *hh* curves is almost negligible for the smooth surface, whereas they are similar, but not identical, for the rough surface. Specifically, the difference never exceeds 5 dB for the rough surface. We conclude that for a rough surface, $\sigma^0_{vv} = \sigma^0_{hh}$, and the magnitude of these two co-polarized coefficients are related to the angle-dependent reflectivity of the surface.

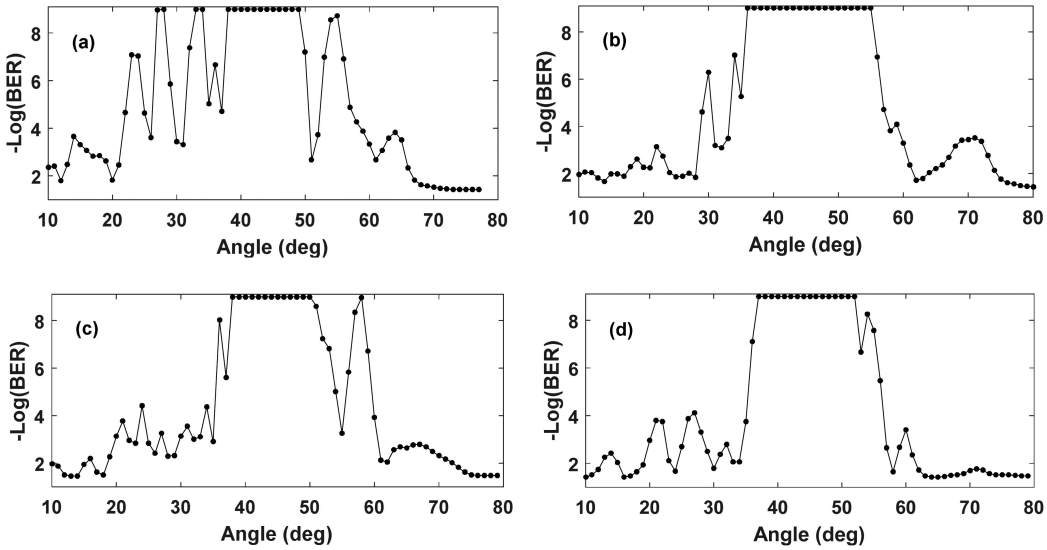

Fig. 4. Measured BER pattern with respect to scattering angle θ_s after reflection by Sample (a) I, (b) II, (c) III, (d) IV when incident angle $\theta_i = 45°$.

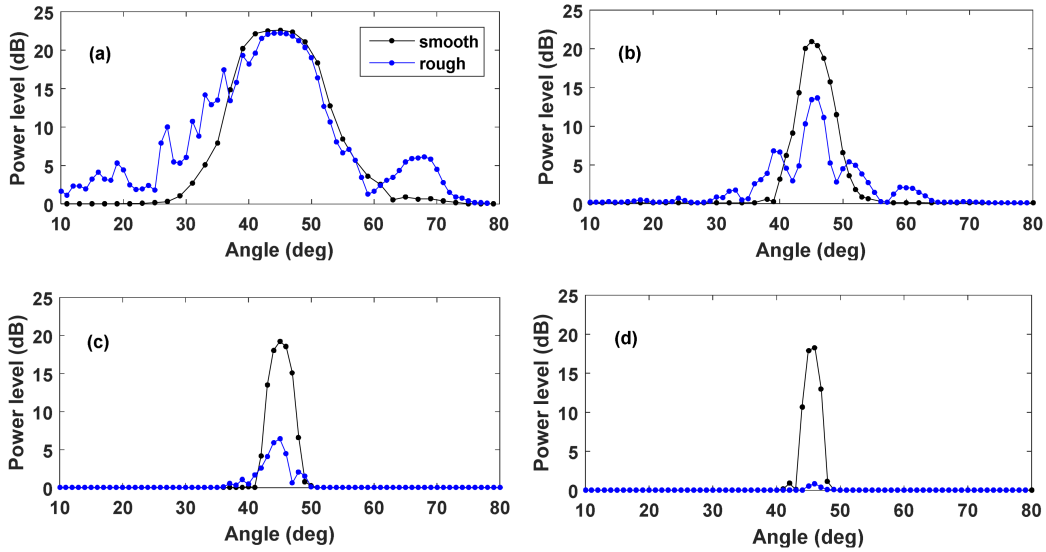

Fig. 5. Measured power pattern as a function of the scattering angle θ_s after reflection by smooth surface (black) and Sample III (blue) for carrier frequency of (a) 100 GHz, (b) 200 GHz, (c) 300 GHz, and (d) 400 GHz.

Fig. 4 displays the angular variation of BER values for *vv* polarization configuration with a 100 GHz data stream reflected by samples I, II, IV, and V. As in Fig. 3, all the patterns are wider than the pattern from a smooth surface. For all the rough surfaces studied here, it is possible to establish an error-free data link at receiver positions (angles,) where no such link would be possible from a smooth surface. These nonspecular paths can be accessed even though the radiated wave from the transmitter is highly directional, due to the incoherent scattering component. We also observe that, in all cases, the reflection from the rough surface introduces perturbations to the beam pattern which resemble interference fringes due to the superposition of the coherent and incoherent waves, as well as diffraction effects (i.e., speckle patterns). This speckle varies in a random fashion as the illuminated area on the rough surface is

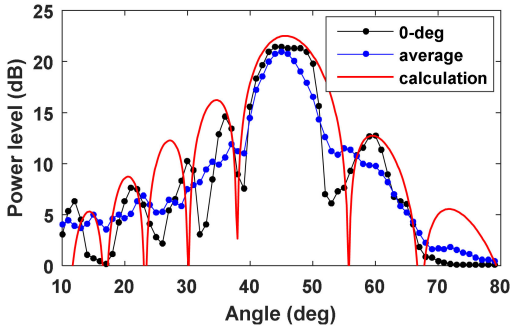

Fig. 6. Comparison between measured (black and blue) and calculated (red) power pattern as a function of the scattering angle θ_s. 0-deg (black) means a single measurement when the rough surface is not rotated; average (blue) means an averaged beam pattern when the rough surface is rotated over 360° with a step of 20°.

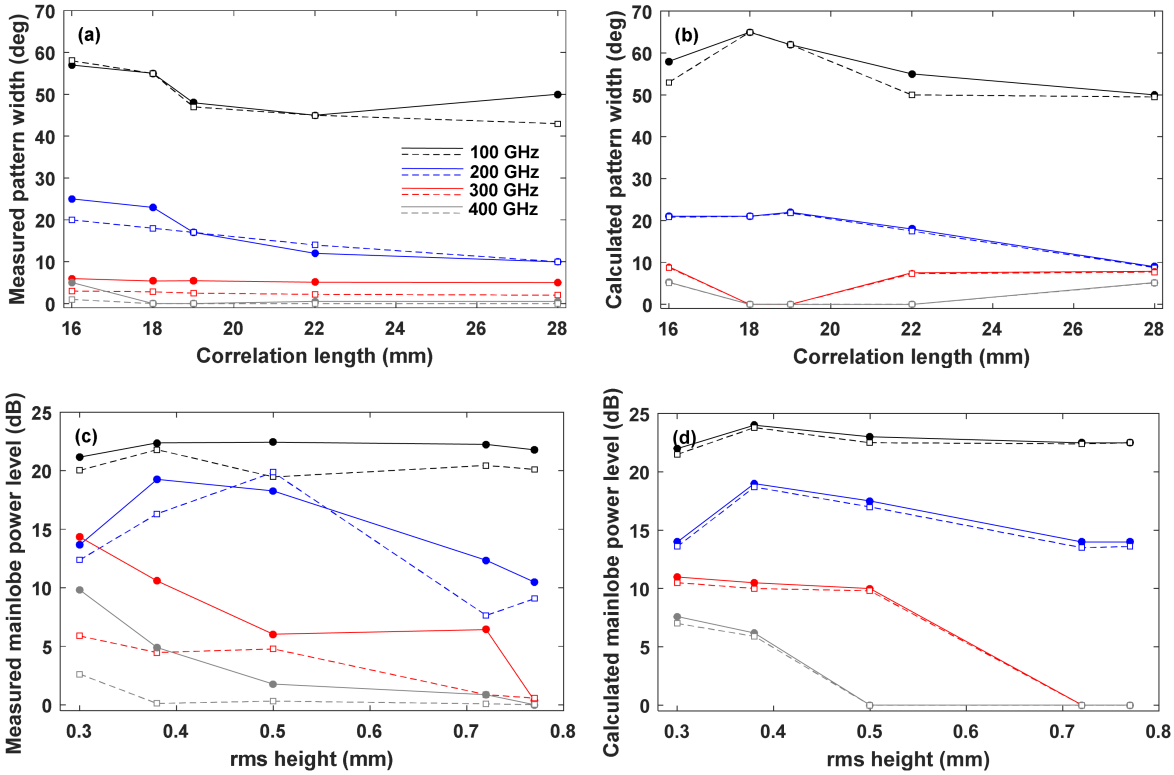

Fig. 7. (a) Measured power pattern width as a function of surface correlation length and (c) main lobe power level versus rms height. And compared with [(b), (d)] theoretical prediction. Filled circles connected by solid lines are for *vv* polarization configuration; open squares connected by dashed lines are for *hh* configuration.

changed, due to the random variation of the surface height profile.

When we increase the carrier frequency, the effective roughness increases because the wavelength becomes smaller compared with the surface texture size, and so the related scattering effect is more pronounced. Fig. 5 illustrates this effect, showing the angular distribution of the scattered power at all four of our carrier frequencies, reflected by sample II. Here, we cannot directly compare the pattern width at different frequencies because of their different divergence angles at the transmitter (see [9]). Instead, we compare the widths to those obtained from a smooth surface, at each frequency. We see that the beam pattern is broadened by rough surfaces at 100 and 200 GHz, in addition to a power loss in the specular direction (main lobe); for example, at 200 GHz the main lobe is decreased by about 6 dB compared to the smooth surface. At higher frequencies, the pattern width becomes narrower, not broader, after reflection by the rough surface, and the loss of power in the main lobe is much larger (around 14 dB at 300 GHz and 18 dB at 400 GHz). In these cases, the redistribution of power from the main lobe (coherent) to the other directions (incoherent) is so large that the signal scattered into the solid angle of the detector is too low to measure at angles outside of the main lobe. The apparent narrowing of the angular pattern is therefore an artifact of the finite dynamic range of our detector. We confirm this result using theoretical predictions based on the IEM model, discussed below.

In Fig. 6, we compare the measured power as a function of the scattering angle to theoretical predictions based on the IEM model discussed above, using sample V and a carrier frequency of 100 GHz. In the calculation, we assume that the rough surface is homogeneous (i.e., that both σ and L_c are constant across the surface). We find that there is a higher discrepancy between the model and measurements, in comparison with earlier work on the characterization of back-scattering from a rough surface [41], although the qualitative behavior is well reproduced. To further investigate this, we measured the beam pattern repeatedly, by rotating the rough surface over 360° with a step of 20° in order to sample different realizations of the randomness. The blue curve in Fig. 6 illustrates the average of these 18 measurements. Here, we see the side lobes characteristic of speckle are suppressed, indicating that these features are characteristic of the specific random distribution.

Based on the above discussion, we conclude that, if the amount of scattering in a multipath environment is large enough, then true NLOS links could be established when both the direct LOS path and specular reflection paths are blocked completely. It is therefore important to understand how the surface parameters which characterize a rough surface can affect the scattering patterns.

Fig. 7(a) and (c) show the evolution of the scattering pattern's angular width (3 dB width above noise level) and main lobe power level with the surface parameters (i.e., correlation length and rms height). The values are set to 0 at several points for the highest carrier frequency (400 GHz), since at this frequency the beam is scattered broadly and the beam power is below the noise level of our detector. The measurements are strikingly similar to

those predicted by the IEM model [see Fig. 7(b) and (d)]. We find that the rms height has the greatest effect on the power level of the main lobe in the specular direction, while the surface height correlation length is more responsible for changes in the width of the scattering pattern. In particular, a larger rms height variation leads to more power loss in the specular direction, and a smaller correlation length results in a larger value for the angular width of the scattering pattern.

V. Conclusion

In this article, the diffuse bistatic scattering response of several metallic rough surfaces were measured using a data stream in the THz frequency range. NLOS paths can either take the form of specular reflection or diffuse nonspecular scattering; both can be valuable for establishing a link when the direct LOS link is blocked. We show that the angular width of the diffuse scattered component is more sensitive to the surface correlation length than to the rms height variation. We compare our results to the predictions of the IEM model for bistatic scattering, and find reasonable agreement with the predictions. We emphasize that these results have been obtained using amplitude-only modulation of the terahertz carrier wave. One might expect somewhat different results if a more complex modulation scheme such as BPSK is used. Even so, it seems plausible that nonspecular NLOS paths can play a valuable role in THz wireless systems, even though the beams are highly directional and the channels are lossy. If a directional LOS link is temporarily blocked by a moving obstruction [6], one can envision that the access point would need to dynamically respond by switching to an NLOS channel in order to maintain the connection. The possibility of using a nonspecular NLOS path, as demonstrated here, would broaden the range of possible options for the access point, and therefore improve the overall link performance.

References

[1] T. Kleine-Ostmann and T. Nagatsuma, "A review on terahertz communications research," *J. Infrared Millim. THz Waves*, vol. 32, pp. 143–171, 2011.

[2] K. Sengupta, T. Nagatsuma, and D. M. Mittleman, "Terahertz integrated electronic and hybrid electronic–photonic systems," *Nature Electron.*, vol. 1, pp. 622–635, 2018.

[3] V. Petrov, J. Kokkoniemi, D. Moltchanov, J. Lehtomaki, Y. Koucheryavy, and M. Juntti, "Last meter indoor terahertz wireless access: Performance insights and implementation roadmap," *IEEE Commun. Mag.*, vol. 56, no. 6, pp. 158–165, Jun. 2018.

[4] H. Elayan, C. Stefanini, R. M. Shubair, and J. M. Jornet, "End-to-end noise model for intra-body terahertz nanoscale communication," *IEEE Trans. NanoBiosci.*, vol. 17, no. 4, pp. 464–473, Oct. 2018.

[5] J. Ma *et al.*, "Security and eavesdropping in terahertz wireless links," *Nature*, vol. 563, pp. 89–93, 2018.

[6] V. Petrov, M. Komarov, D. Moltchanov, J. M. Jornet, and Y. Koucheryavy, "Interference and SINR in millimeter wave and terahertz communication systems with blocking and directional antennas," *IEEE Trans. Wireless Commun.*, vol. 16, no. 3, pp. 1791–1808, Mar. 2017.

[7] M. Koch, "Terahertz communications: A 2020 vision," in *Terahertz Frequency Detection and Identification of Materials and Objects*, R. E. Miles, X.-C. Zhang, H. Eisele, and A. Krotkus, Eds., Berlin, Germany: Springer, 2007, pp. 325–338.

[8] B. Peng, S. Rey, and T. Kürner, "Channel characteristics study for future indoor millimeter and submillimeter wireless communications," in *Proc. 10th Eur. Conf. Antennas Propag.*, Davos, Switzerland, 2016, doi: 10.1109/EuCAP.2016.7481456.

[9] J. Ma, R. Shrestha, L. Moeller, and D. M. Mittleman, "Channel performance for indoor and outdoor terahertz wireless links," *APL Photon.*, vol. 3, 2018, Art. no. 051601.

[10] S. Y. Seidel, T. S. Rappaport, S. Jain, M. L. Lord, and R. Singh, "Path loss, scattering, and multipath delay statistics in four European cities for digital cellular and microcellular radiotelephone," *IEEE Trans. Veh. Technol.*, vol. 40, no. 4, pp. 721–730, Nov. 1991.

[11] T. S. Rappaport, "Characterization of UHF multipath radio channels in factory buildings," *IEEE Trans. Antennas Propag.*, vol. 37, no. 8, pp. 1058–1069, Aug. 1989.

[12] O. Landron, M. J. Feuerstein, and T. S. Rappaport, "In situ microwave reflection coefficient measurements for smooth and rough exterior wall surfaces," presented at the IEEE 43rd Veh. Technol. Conf., Secaucus, NJ, USA, 1993, pp. 77–80.

[13] T. S. Rappaport, G. R. MacCartney, S. Sun, H. Yan, and S. Deng, "Small-scale, local area, and transitional millimeter wave propagation for 5G communications," *IEEE Trans. Antennas Propag.*, vol. 65, no. 12, pp. 6474–6490, Dec. 2017.

[14] A. Maltsev, R. Maslennikov, A. Sevastyanov, A. Khoryaev, and A. Lomayev, "Experimental investigations of 60 GHz WLAN systems in office environment," *IEEE J. Sel. Areas Commun.*, vol. 27, no. 8, pp. 1488–1499, Oct. 2009.

[15] G. R. Maccartney, T. S. Rappaport, S. Sun, and S. Deng, "Indoor office wideband millimeter-wave propagation measurements and channel models at 28 and 73 GHz for ultra-dense 5G wireless networks," *IEEE Access*, vol. 3, pp. 2388–2424, 2015.

[16] T. S. Rappaport, E. Ben-Dor, J. N. Murdock, and Y. Qiao, "38 GHz and 60 GHz angle-dependent propagation for cellular & peer-to-peer wireless communications," presented at the IEEE Int. Conf. Commun., 2012, pp. 4568–4573.

[17] T. S. Rappaport, G. R. MacCartney, M. K. Samimi, and S. Sun, "Wideband millimeter-wave propagation measurements and channel models for future wireless communication system design," *IEEE Trans. Commun.*, vol. 63, no. 9, pp. 3029–3056, Sep. 2015.

[18] S. Sun, G. R. MacCartney, and T. S. Rappaport, "Millimeter-wave distance-dependent large-scale propagation measurements and path loss models for outdoor and indoor 5G systems," in *Proc. 10th Eur. Conf. Antennas Propag.*, Davos, Switzerland, 2016, doi: 10.1109/EuCAP.2016.7481506.

[19] Z. Jian, J. Pearce, and D. M. Mittleman, "Characterizing individual scattering events by measuring the amplitude and phase of the electric field diffusing through a random medium," *Phys. Rev. Lett.*, vol. 91, 2003, Art. no. 033903.

[20] J. Pearce, Z. Jian, and D. M. Mittleman, "Statistics of multiply scattered broadband terahertz pulses," *Phys. Rev. Lett.*, vol. 91, 2003, Art. no. 043903.

[21] C. Jansen *et al.*, "Diffuse scattering from rough surfaces in THz communication channels," *IEEE Trans. THz Sci. Technol.*, vol. 1, no. 2, pp. 462–472, Nov. 2011.

[22] E. N. Grossman, N. Popovic, R. A. Chamberlin, J. Gordon, and D. Novotny, "Submillimeter wavelength scattering from random rough surfaces," *IEEE Trans. THz Sci. Technol.*, vol. 7, no. 5, pp. 546–562, Sep. 2017.

[23] R. Piesiewicz, C. Jansen, D. M. Mittleman, T. Kleine-Ostmann, M. Koch, and T. Kürner, "Scattering analysis for the modeling of THz communication systems," *IEEE Trans. Antennas Propag.*, vol. 55, no. 11, pp. 3002–3009, Nov. 2007.

[24] S. Ju *et al.*, "Scattering mechanisms and modeling for terahertz wireless communications," in *Proc. IEEE Int. Commun. Conf.*, Shanghai, China, 2019, doi: 10.1109/ICC.2019.8761205.

[25] A. K. Fung, W. Y. Liu, K. S. Chen, and M. K. Tsay, "An improved IEM model for bistatic scattering from rough surfaces," *J. Electromagn. Waves Appl.*, vol. 16, pp. 689–702, 2002.

[26] P. Beckmann and A. Spizzichino, *The Scattering of Electromagnetic Waves from Rough Surfaces*, Norwood, MA: Artech House, 1987.

[27] A. K. Fung, *Microwave Scattering and Emission Models and Their Applications*. Norwood, MA, USA: Artech House, 1994.

[28] F. T. Ulaby, R. K. Moore, and A. K. Fung, *Microwave Remote Sensing: Active and Passive, Vol. I: Radar Remote Sensing and Surface Scattering and Emission Theory*. Reading, MA, USA: Addison-Wesley, 1982.

[29] J. He, T. Yu, N. Geng, and L. Carin, "Method of moments analysis of electromagnetic scattering from a general three-dimensional dielectric target embedded in a multilayered medium," *Radio Sci.*, vol. 35, pp. 305–313, 2000.

[30] J. M. Bourgeois and G. S. Smith, "A fully three-dimensional simulation of a ground-penetrating radar: FDTD theory compared with experiment," *IEEE Trans. Geosci. Remote Sens.*, vol. 34, no. 1, pp. 36–44, Jan. 1996.

[31] R. F. Harrington, *Field Computation by Moment Methods*. Hoboken, NJ, USA: Wiley, 1993.
[32] V. Degli-Esposti, D. Guiducci, A. de'Marsi, P. Azzi, and F. Fuschini, "An advanced field prediction model including diffuse scattering," *IEEE Trans. Antennas Propag.*, vol. 52, no. 7, pp. 1717–1728, Jul. 2004.
[33] J. E. Harvey, "Modified Beckmann-Kirchhoff scattering model for rough surfaces with large incident and scattering angles," *Opt. Eng.*, vol. 46, 2007, Art. no. 078002.
[34] A. K. Fung, Z. Li, and K. S. Chen, "Backscattering from a randomly rough dielectric surface," *IEEE Trans. Geosci. Remote Sens.*, vol. 30, no. 2, pp. 356–369, Mar. 1992.
[35] J. L. Álvarez-Pérez, "An extension of the IEM/IEMM surface scattering model," *Waves Random Media*, vol. 11, pp. 307–329, 2009.
[36] J. L. Álvarez-Pérez, M. Vall-llossera, and J. C. Nieto-Borge, "Emissivity calculations for two-dimensional ocean surfaces with the improved integral equation model IEM2M," presented at the IEEE Int. Symp. Geosci. Remote Sens., Denver, CO, USA, 2006, pp. 473–476.
[37] J. C. Wei, H. Chen, X. Qin, and T. J. Cui, "Surface and volumetric scattering by rough dielectric boundary at terahertz frequencies," *IEEE Trans. Antennas Propag.*, vol. 65, no. 6, pp. 3154–3161, Jun. 2017.
[38] M. A. Ordal, R. J. Bell, R. W. Alexander, L. L. Long, and M. R. Querry, "Optical properties of fourteen metals in the infrared and far infrared: Al, Co, Cu, Au, Fe, Pb, Mo, Ni, Pd, Pt, Ag, Ti, V, and W," *Appl. Opt.*, vol. 24, pp. 4493–4499, 1985.
[39] H.-J. Hagemann, W. Gudat, and C. Kunz, "Optical constants from the far infrared to the x-ray region: Mg, Al, Cu, Ag, Au, Bi, C, and Al2O3," *J. Opt. Soc. Am. A*, vol. 65, pp. 742–744, 1975.
[40] H. U. Yang, J. D'Archangel, M. L. Sundheimer, E. Tucker, G. D. Boreman, and M. B. Raschke, "Optical dielectric function of silver," *Phys. Rev. B*, vol. 91, 2015, Art. no. 235137.
[41] A. Y. Nashashibi and F. T. Ulaby, "MMW polarimetric radar bistatic scattering from a random surface," *IEEE Trans. Geosci. Remote Sens.*, vol. 45, no. 6, pp. 1743–1755, Jun. 2007.

Jianjun Ma received the Ph.D. degree in applied physics from the New Jersey Institute of Technology, Newark, NJ, USA, in 2015, under the guidance of Prof. John F. Federici. His Ph.D. dissertation was about the weather impacts on outdoor terahertz and infrared wireless communication links.

In 2016, he joined Prof. Daniel M. Mittleman's group at Brown University, RI, USA, as a Postdoctoral Research Associate. In 2019, he joined the Beijing Institute of Technology, Beijing, China, as a Professor. His current research interests include terahertz wireless communications, terahertz time domain detection, terahertz waveguides, terahertz indoor/outdoor propagation, and link security.

Rabi Shrestha received the B.S. degree in electrical and computer engineering and the M.S. degree in electrical engineering from the University of Rochester, Rochester, NY, USA, in 2016 and 2017, respectively. He is currently working toward the Ph.D. degree in Brown University, Providence, RI, USA, under the guidance of Prof. Daniel M. Mittleman.

His current research interests include terahertz wireless communication and technology.

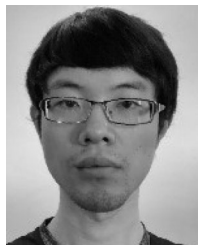

Wei Zhang received the B.S. degree in electrical engineering from Peking University, Beijing, China, in 2014. He is currently working toward the Ph.D. degree in Brown University, Providence, RI, USA.

His current research interests include all aspects of terahertz science and technologies, as well as general photonics.

Lothar Moeller received the Dipl. Phys. degree in physics and the Dipl. Ing. degree in electrical engineering from RWTH Aachen, Aachen, Germany, in 1992 and 1993, respectively, and the Ph.D. degree in electrical engineering from ETH Zurich, Zurich, Switzerland, in 1996.

He joined Bell Labs in 1997 where he researched and developed novel modulation and equalization techniques for a variety of technology fields including optical fiber transmission, THz communication systems with ultrahigh capacity, THz security scanners, and detection of cell phone radiation using MRI. Since 2014, he has been with the R&D division of TE Connectivity, where he focuses on undersea telecommunication systems. He became a Research Professor with the New Jersey Institute of Technology and a Guest Professor with the Shanghai Jiao Tong University, in 2014 and 2005, respectively.

Daniel M. Mittleman (F'11) received the B.S. degree in physics from the Massachusetts Institute of Technology, in 1988, and the M.S. degree in physics from the University of California, Berkeley, Berkeley, CA, USA, in 1990, and the Ph.D. degree in physics from the University of California, Berkeley, in 1994, under the direction of Dr. Charles Shan.

He then joined the AT&T Bell Laboratories as a postdoctoral member of the technical staff, working first for Dr. Richard Freeman on a terawatt laser system, and then for Dr. Martin Nuss on terahertz spectroscopy and imaging. He joined the ECE Department at Rice University in September 1996. In 2015, he moved to the School of Engineering at Brown University. His research interests involve the science and technology of terahertz radiation.

Dr. Mittleman is a Fellow of the OSA, and the APS, and was a 2018 recipient of the Humboldt Research Award. He currently serving a three-year term as Chair of the International Society for Infrared Millimeter and Terahertz Waves.